

CAPTURING VORTEX ENERGY FROM THE FLOW ON THE AHMED CAR

Louis Gagnon, louis.gagnon.10@ulaval.ca
Marc J. Richard, marc.richard@gmc.ulaval.ca
Benoît Lévesque, benoit.levesque@gmc.ulaval.ca
Dept. of Mechanical Engineering
Laval University
Québec (Québec) Canada

Abstract. *A two-dimensional numerical analysis of the Ahmed body was performed using the k - ω -SST turbulence model implemented in the OpenFOAM software. The analysis was then modified to include a rotating paddle wheel which captures energy from the swirl that forms behind the vehicle. The rotating wheel is modeled using a General Grid Interface (GGI) and the energy captured is calculated with the help of the forces library of the OpenFOAM software. Power generation reaches 16.1 watts at optimal conditions. Drag reductions up to 8.2% were also found as side-effects of the rotating paddle wheel. Most computations are run in parallel on a dual core computer. A mesh of 30,000 cells is used. Y^+ values on the walls of the vehicle go from 60 to 500. Tests are run at both fixed and variable rotating velocities. Calculations usually reach a steady state (in average) after 0.2 to 0.3 seconds. The Ahmed body is subjected to a flow velocity of 60 m/s and that velocity is used to calculate the equivalent power demand of the drag coefficient. It was found that there is a specific range of rotational velocities that yield the best power output and that range is determined by the rotational velocity of the vortex. The wheel has to be located within the rear separation bubble to avoid increasing the drag on the car by locating the wheel into the free-stream flow. An algorithm is currently being developed to have the rotational velocity of the paddle wheel regulated by the flow in a manner where the energy harvested would be dependent on the magnitude of the force moment acting on the paddle wheel; that would smoothen the cyclic variations of power generated by the paddle wheel. In a practical application, the energy captured would be converted into electricity which has the double advantage of allowing an electric motor to regulate the rotational velocity according to calculated and/or measured quantities and sending the power directly to an on-board hybrid electric battery system, which is becoming more and more available in today's vehicles. The paddle wheel system would have its most beneficial impact on vehicles that are involved in a lot of highway driving, where the forces of wind are at their maximum.*

Keywords: *Ahmed body, drag coefficient, energy capture, rotating interface, OpenFOAM.*

1. INTRODUCTION

The aerodynamics of turbulent flows remains a subject of both great interest and great challenge to engineers. Many questions still remain unanswered, and consequently many opportunities for development still remain unexplored. Aerodynamics are an important aspect of most design projects the reason often being to build safe structures that will resist the strongest winds. Other times it is important to evaluate aerodynamics to ensure that flow-cooled parts of a system will be cooled properly. However, an aspect that has also fascinated many engineers since the dawn of engine-powered travel is the external aerodynamics of vehicles: the resistance of wind to the forward movement of a car, bus, train, etc.. A large portion of the energy consumed by ground vehicles is used to overcome pressure drag. In fact, the scientific community still questions whether the optimal drag reduction on a body would equate to a null pressure drag. In an attempt to bring new ideas to the table, this paper shows how moving parts can be added to an automobile model to reduce the energy it consumes to overcome wind resistance. That is achieved by capturing energy from the swirls and modifying the flow that exists behind a hatchback car. The energy is captured by a rotating device located within the separation bubble of the flow behind the vehicle. The moving parts in question are inspired by paddle wheels and their purpose is to recapture energy from the vortices located behind a moving vehicle. Although the simulations were performed on a car model, tractor-trailer rigs would be ideal candidates for the type of energy capture presented in this paper, as well as any vehicle involved in a lot of highway driving.

2. THE CAR MODEL

The Ahmed car model was chosen as the shape to analyze in the simulations because it has received widespread attention from the scientific community since its first appearance when Ahmed, Ramm and Faltin (1984) used it in a wind tunnel to mimic the flow found around a typical car. This model was also chosen by the European Research Community On Flow, Turbulence, And Combustion (ERCOTAC) to benchmark different Computational Fluid Dynamics (CFD) codes. The first goal of this study was thus to create a CFD case that would reproduce the generally accepted flow characteristics of the Ahmed body and, most important, its drag coefficient with a minimal error. Reproducing the experimental drag

coefficient of the Ahmed body has been a challenge for many researchers that studied the Ahmed body because of the difficulty to precisely locate the start and end of the separation bubble on the rear slant wall of the body. However, a general idea of the appropriate drag coefficient was grasped from the published research to be in the range of 0.25 to 0.35 when the rear slant angle is 25°. It must also be pointed out that between the two widely used angles of 25° and 35° there is a drag crisis. The crisis occurs at roughly 30° and is characterized by the experimental drag coefficient reaching 37.8 (Ahmed, Ramm and Falin, 1984). Several attempts were done by different authors to reproduce the transition phenomenon that occurs between those two angles where the flow actually goes from having its longitudinal (stream-wise) vortices form on the sides of the rear slant wall of the vehicle to having them start only on the lower, vertical, rear end. Those vortices have a significant influence on the three-dimensional drag on the Ahmed body because they interact with the separation bubble located on the slant wall. However, Beaudoin and Aider (2008) have experimentally demonstrated that those vortices could be avoided by use of side wings on the slant wall of the model and that removing them can also reduce drag. Lehugeur, Gilliéron, and Ivanić (2006) also reduced drag when breaking down stream-wise vortices and reducing their vorticity by 75% by blowing at the location where Beaudoin and Aider (2008) had installed side wings. The goal of this project is to deal with the middle, two-dimensional, separation bubble which exists behind the body and hosts two span-wise vortices that meet approximately in the middle of the rear vertical wall of the car. The kinetic energy of these vortices is what is recaptured by the paddle wheels used in this paper.

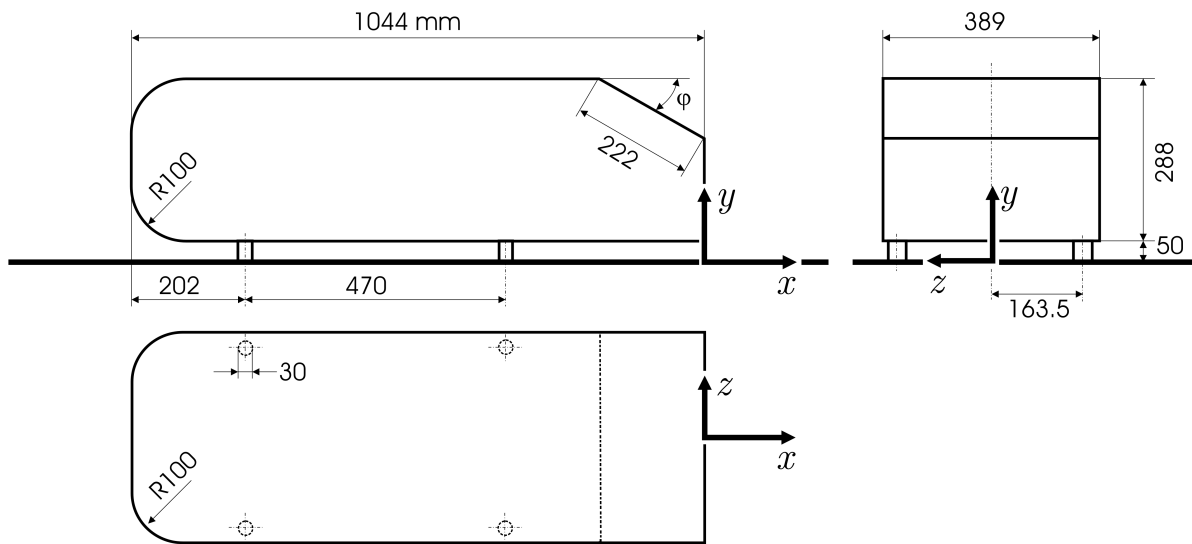


Figure 1. The Ahmed body, adapted from (Hinterberger, García-Villalba and Rodi, 2004) with kind permission of Springer Science+Business Media. Throughout this paper, the x, y, z axes represent stream-wise, vertical, and span-wise directions, respectively.

3. CFD ANALYSIS

3.1 Governing Equations

The OpenFOAM solver «turbDyMFoam», which is used for all the calculations presented, uses an unsteady flow model. One can notice that the density ρ does not appear in the incompressible fluid equations and thus the results of pressure found are actually pressure divided by density. The Navier-Stokes equations are solved within a PISO loop. Turbulence is incorporated into RANS equations using the following equation,

$$\frac{\partial \mathbf{U}}{\partial t} + \nabla \cdot \phi \mathbf{U} = -\nabla p + \nabla \cdot \nu_{eff} \nabla \mathbf{U} + \nabla \cdot (\nu_{eff} ((\nabla \mathbf{U})^T - \frac{1}{3} (\nabla \cdot \mathbf{U}) \mathbf{I})) \quad (1)$$

where the effective turbulent viscosity is

$$\nu_{eff} = \nu_t + \nu \quad (2)$$

Now the turbulence model comes in and it is described below.

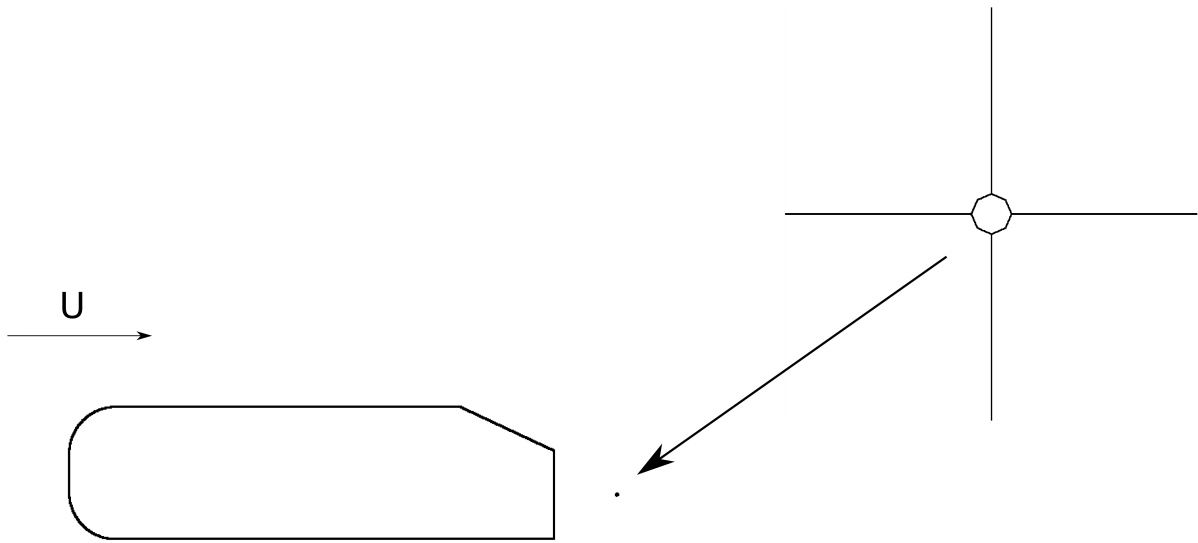


Figure 2. The two-dimensional representation of the Ahmed body with the paddle wheel located behind its rear vertical wall.

3.2 Turbulence model

Large Eddy Simulations (LES) models were considered but not deemed appropriate for two-dimensional modeling even if some authors have reported successful use of LES in two dimensions (Bouris and Bergeles, 1999). Reports of Unsteady Reynolds-Averaged Navier Stokes equations (URANS) models yielding reasonably accurate drag coefficients of the Ahmed body are available in the literature (Guilmineau, 2008); however, Guilmineau also reports an incapability of the model to properly reproduce the experimental flow on the rear slant wall that detaches and quickly reattaches when at a 25° slant angle. The k - ω -SST model features an automatic wall treatment and uses k - ω equations within the boundary layer and k - ϵ equations in the free-stream flow; a blending function ensures a smooth transition between the near wall and free-stream equations. Considering that Bayraktar found good results using the RNG k - ϵ model on the Ahmed body (Bayraktar, Landman and Baysal, 2001), use of k - ϵ equations in the free-stream flow should give reliable results.

According to the k - ω -SST turbulence model, the turbulent viscosity, ν_t , is

$$\nu_t = \frac{a_1 k}{\max(a_1 \omega, F2 \sqrt{S2})} \quad (3)$$

where a_1 , $F2$, and $S2$ are defined by OpenCFD (2009).

The turbulent kinetic energy, k , and turbulent frequency, ω , are solved by,

$$\frac{\partial k}{\partial t} + \nabla \cdot (\mathbf{U}k) = \min(G, c_1 \beta^* k \omega) - \beta^* \omega k + \nabla \cdot (\alpha_k \nu_t + \nu) \nabla k \quad (4)$$

$$\frac{\partial \omega}{\partial t} + \nabla \cdot (\mathbf{U}\omega) = 2\gamma S2 - \beta \omega^2 + \nabla \cdot (\alpha_\omega \nu_t + \nu) \nabla \omega - ((F1 - 1) \frac{(2\alpha_\omega \omega (\nabla k \cdot \nabla \omega))}{\omega}) \quad (5)$$

where the values of the undefined constants are given by OpenCFD (2009). The reader is also encouraged to see the paper by Menter and Esch (2001) which mathematically describes the k - ω -SST turbulence model.

3.3 Parameters and boundary conditions

The air velocity used in the analysis is $U = 60 \text{ m/s}$ and the kinematic viscosity is $\nu = 14.75 \times 10^{-6} \text{ m}^2/\text{s}$. The Reynolds number of this analysis, based on model length, is $Re = 4.25 \times 10^6$. k and ω inlet boundary conditions are based on a 0.5% turbulence intensity (Ahmed, Ramm and Falin, 1984) and an approximated turbulent length scale of 5 cm. The slant angle is 25° .

3.4 Mesh

A Reynolds number of 4.25×10^6 requires a very fine mesh. Due to the chaotic behavior of the flow close to the body, a structured boundary layer mesh is only used at locations of very small tangential gradient of the near-wall flow properties. Thus, only two small zones of the mesh are structured and use about 500 less cells than an equivalent unstructured mesh. Using a boundary layer mesh on the front of the body is not appropriate because the pressure gradient is as strong along the tangent of the surface as along the normal. Using a structured mesh on the rear slant and vertical surfaces is also inappropriate due to sudden changes in pressure at specific locations and a velocity distribution typical of detached flows. It is also necessary to have a well resolved mesh behind the car to properly simulate the wake. The mesh on the wall of the vehicle requires a fine resolution because of its influence on the drag coefficient. The zone just upstream of the vehicle is meshed slightly coarser than the wake because there are no vortices in front of the car: only a saddle point affects the out-of-boundary-layer upstream flow. Considering that it is generally recommended to have at least 15 nodes in the boundary layer and that the flat plate boundary layer thickness is estimated to be 2 cm (Cousteix, 1989), it is not possible to precisely resolve the said layer and the simulations rely on wall models from the solver.

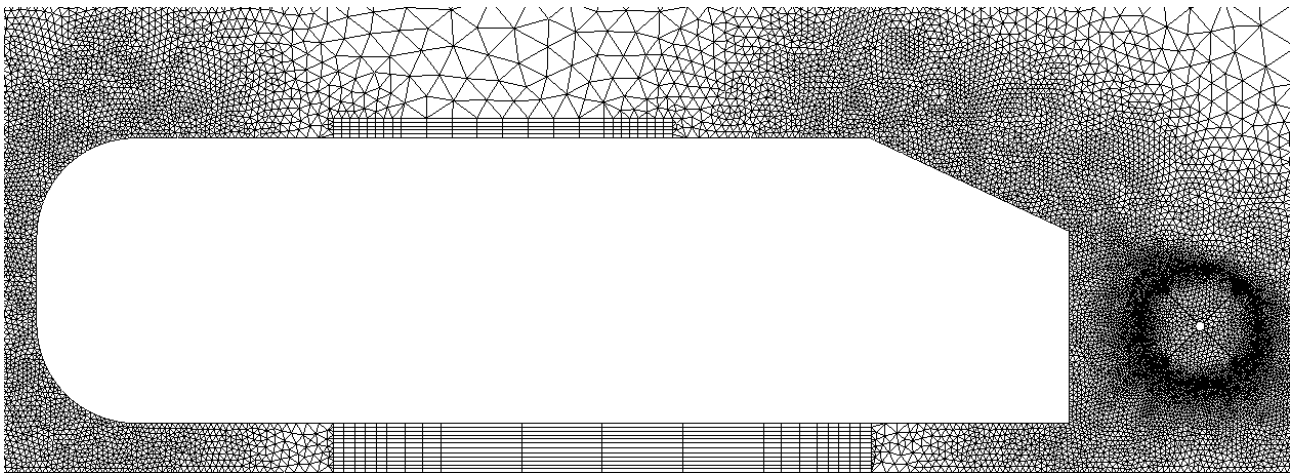


Figure 3. Mesh of the vehicle.

In their three-dimensional numerical analysis of the Ahmed body, Bayraktar, Landman, and Baysal (2001) found from mesh refinement tests that a 4.4M cells unstructured mesh yields a fine correlation between experimental and numerical drag coefficients. From that number of cells and the assumption that the relative numbers of cells in the longitudinal, lateral, and vertical directions are a , $0.25a$, and $0.2a$, respectively, it was found using the following equation that an equivalent 2D mesh would have 40K cells,

$$a \times 0.2a \times 0.25a = 4.4 \times 10^6 \implies a = 444.80 \quad \therefore N_{cells,2D} = a \times 0.2a \approx 40000 \quad (6)$$

where a is the unknown and $N_{cells,2D}$ is the number of cells of the equivalent two-dimensional mesh. The meshes used for the present analysis are slightly rougher and have 27.5K to 34K cells. All meshes are generated by the Gmsh software.

3.5 Rotating interface

The General Grid Interface (GGI) of the OpenFOAM software is used to allow the paddle wheel to rotate with respect to the car. This is accomplished by having the solver interpolate the face values of the flow properties at a virtual interface which is indicated to the solver by the definition of two coincident circles that delimit the inner (rotating part) and outer (fixed car) parts of the mesh. Details of this approach are given by OpenCFD (2009). As seen in Fig. 3, the mesh resolution at the interface, to the right of the car, is increased in order to make the interface as close as possible to a perfect circle and reduce to a minimum the empty zones that exist between the inner and outer parts of the mesh. Those zones cause divergence of the solution when they become too large.

3.6 Validation

The drag coefficient of the unaltered two-dimensional Ahmed body simulation is used to calculate the drag coefficient differences between the energy-capturing and the reference (unaltered) models. It is thus necessary to have a certain level of confidence towards the solution of the flow around that particular body. This level of assurance is gained by running a mesh refinement test with a mesh that contains twice as many nodes in each direction. The refined mesh has 111.5K

cells. A fairly accurate (6% difference) correlation between the drag coefficients of both meshes is found. The simulation with the finer mesh yields a slightly higher drag coefficient, that makes the calculation of total drag reduction by use of the paddle wheel more conservative. The flow fields of the refined mesh give a more detailed view of the flow properties but both analyses share the same general flow characteristics.

A time-step of 1×10^{-5} second is used for the simulations that use the reference mesh. The simulations with the added paddle wheel have a roughly equal time step. The Courant number, Co , serves as a variable to maintain time steps below a value where divergence could occur. It is defined in the following equation,

$$Co = \frac{\delta t |U|}{\delta x} \quad (7)$$

where δt is the time step, δx is the length of the cell in the direction of the flow, and $|U|$ is the magnitude of the velocity through the cell in question.

In the paddle wheel case, time steps are automatically adjusted so that $Co \leq 0.5$, which ensures calculation stability by preventing fluid from traveling more than half a cell between each time step (OpenFOAM, 2008). The Courant number is computed for each cell at each time step and the next time step is adjusted according to the maximum Courant number computed.

4. ENERGY CAPTURE

As mentioned in the introduction, the goal is to have an added part that captures energy from the flow. For results to be interesting the total drag with the added part cannot be higher than that of the unaltered Ahmed body. Alternatively, if the total drag is increased then the energy captured from the flow has to surpass the energy lost to drag. To compare energy captured and drag coefficients, the following equation measures of how much power is required to overcome a specific drag coefficient at the traveling velocity of the car,

$$e_{drag} = \left(\frac{1}{2} \times \rho U^2 A C_D \right) \times U \quad (8)$$

where A is the frontal area of the three-dimensional Ahmed body: 0.11203 m^2 and e_{drag} is the drag coefficient converted in Watts. The following equation gives how much power is extracted from the flow,

$$e_{capture} = M_z \times \frac{R \times 2\pi}{60} \times \frac{w}{T} \quad (9)$$

where U is the velocity of the car and of the free-stream flow, M_z is the moment around the z-axis, $e_{capture}$ is the power captured in Watts, and ρ is the density of the ambient air: 1.2 kg/m^3 . R is the rotational velocity of the paddle wheel in revolutions per minute (RPM) and C_D is the drag coefficient considered for conversion into equivalent energy. w is the width of the three-dimensional Ahmed body and T is the thickness of the two-dimensional model used in the analysis: 0.01 m^2 . Old fashion paddle wheels are the source of inspiration for the design. Every wheel discussed in this report has 4 paddles. A constant rotational velocity of the wheel is imposed and the quantity of power generated is calculated from the average of moments acting on the paddle wheel over a chosen number of cycles. Some tests are run with a sinusoidal angular velocity. In a practical application, a generator could control velocity fluctuations by giving power to or taking power from the wheel.

5. RESULTS

In the results, $C_{D,power}$ is the energy saved by the avoided drag when vehicle travels at 60 m/s. The reference case gives a $C_{D,body}$ of 0.300 and that value is used to quantify the amount of drag saved by the various configurations. From Eq. (8), the reference $C_{D,body} = 0.3$ requires 4.36 kW when the three-dimensional Ahmed car is moving at 60m/s. $C_{D,saved}$ is the coefficient of the avoided drag and is defined in the following equation,

$$C_{D,saved} = 0.3 - C_{D,body} - C_{D,part} \quad (10)$$

where $C_{D,body}$ and $C_{D,part}$ represent the drag coefficients on the Ahmed body and on the added part, respectively.

5.1 Selected cases

5.1.1 Fixed rotational velocity

Results from cases of rotating paddle wheels are compiled in Tab. 1. The wheel's center of rotation y-position is 19 cm below the top wall of the body. x_{center} is the distance in cm between the rear vertical wall and the center of the paddle wheel and R is its rotational velocity in RPM. r is the radius of the paddle wheel in cm.

Table 1. Results from selected cases with fixed rotational velocity.

Case	1	2	3	4	5	6
x_{center}	13.3	16.6	13.3	16.6	13.3	13.3
r	5	4	5	4	4	5
R	2500	2000	2000	4000	2000	2300
$C_{D,body}$	0.3084	0.2939	0.3122	0.2954	0.3130	0.3122
$C_{D,part}$	-0.0323	-0.0148	-0.0335	-0.0207	-0.0353	-0.0334
$C_{D,saved}$	0.0240	0.0209	0.0213	0.0252	0.0227	0.0213
$C_{D,power}$	348	304	309	366	324	309
$e_{capture}$	0.9	8.2	12.8	-4.6	6.0	10.4

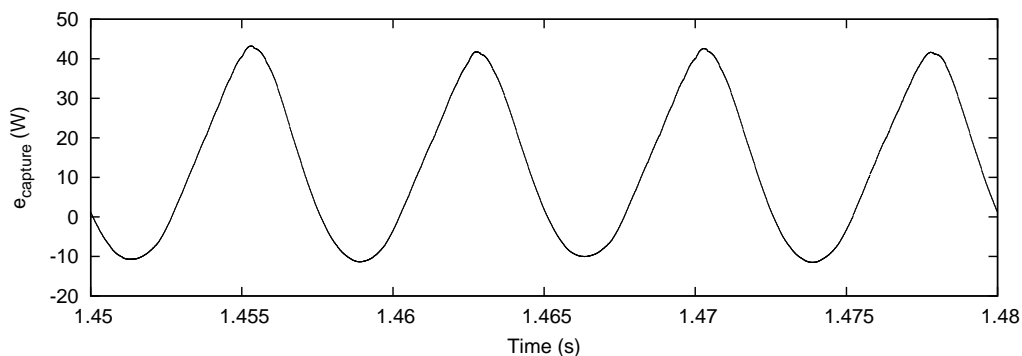


Figure 4. Plot of $e_{capture}$ vs Time for one full revolution of the paddle wheel from case 3.

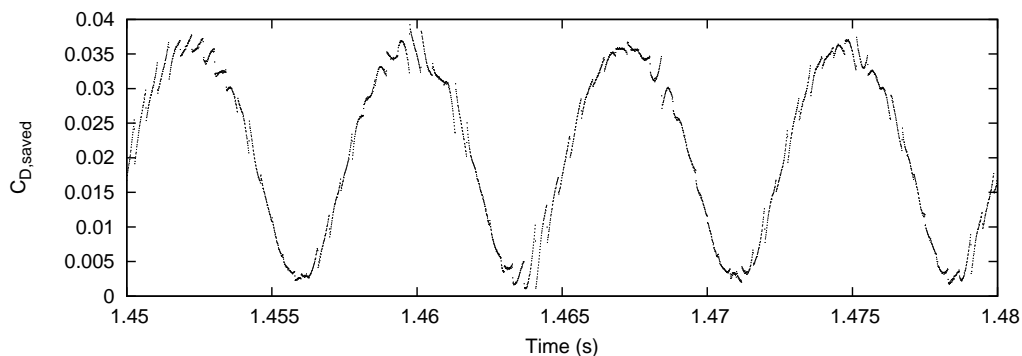


Figure 5. Plot of $C_{D,saved}$ vs Time for one full revolution of the paddle wheel from case 3.

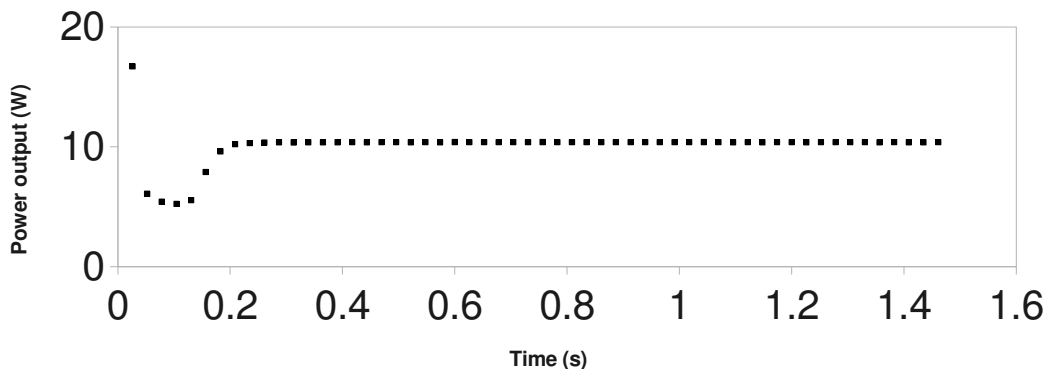


Figure 6. Plot of power output vs time calculated per paddle wheel revolution starting at $t = 0$. Each cycle is 0.0261 seconds long based on the rotational velocity of 2300 RPM. Data taken from case 6.

Figures 4 and 5 illustrate the energy captured and the drag coefficient avoided, respectively, for a full revolution of the paddle wheel of case 3. The data is taken from $t = 1.45s$ to $t = 1.48s$. To illustrate how the flow stabilizes in the first tenths of a second of the simulation, the average power extracted from case 6 is plotted against time in Fig. 6 where each calculation is done for one full revolution of the paddle wheel: 4 geometric cycles. After time $t = 0.26s$ the average power extracted stabilizes at $e_{capture} = 10.38 \pm 0.01W$. Figure 7 shows that most power is generated by the front part of the paddle and thus a more streamline shape for the rear of the paddle would likely increase the resulting power generation. The power cycle is depicted for one paddle but is identical for each of the four paddles; their cycles are each out of phase by 90° due to their geometrical arrangement.

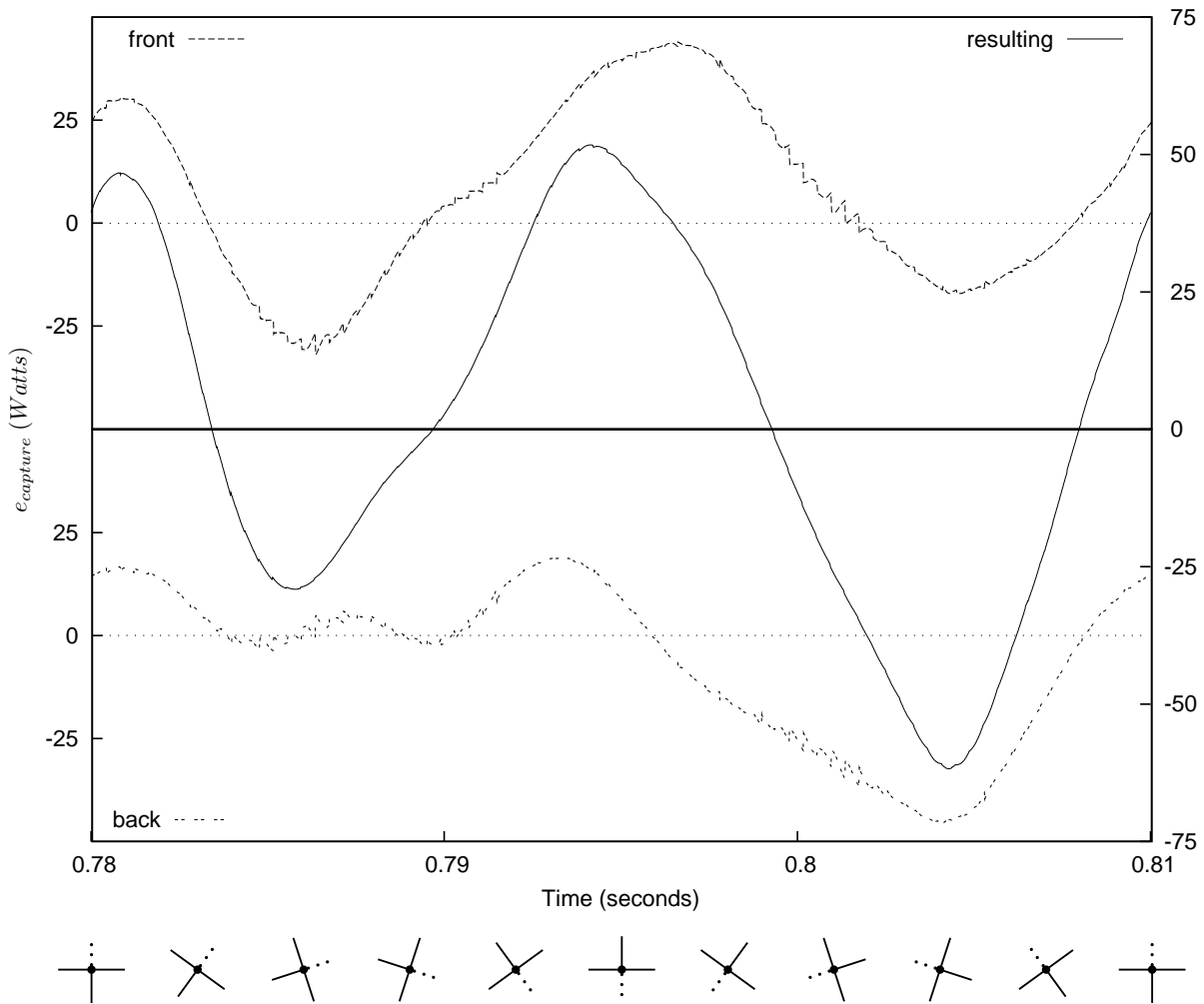


Figure 7. Plot of $e_{capture}$ vs Time for one paddle, depicted below the graph. The left y-axis serves for the front and the back of the paddle and the right y-axis serves for the resulting power generated by that same paddle. Data taken from case 3.

5.1.2 Variable rotational velocity

The OpenFOAM GGI code was modified to allow the wheel to rotate according to a sinusoidal function. Results from two such cases are compiled in Tab. 2 and they are both identical to case 3, with the exception that they have a variable angular velocity. Their angular velocities, R_{var} , are defined by the following equations,

$$R_{var,7} = R \times (1.0 + 0.2 \times \sin(-2.9249 + \frac{R \times \pi}{7.5} \times t)) \quad (11)$$

$$R_{var,8} = R \times (1.0 + 0.2 \times \sin(-2.3 + \frac{R \times \pi}{7.5} \times t)) \quad (12)$$

where R is the base rotational velocity, which is 2000 RPM for both cases, and t is time in seconds. Since the energy production has a period exactly equal to a fourth of the period of oscillation of the paddle wheel, the frequency of the

sinusoidal function is also chosen as such. The only difference between the two cases is the phase angle of the sinusoidal function. $R_{var,7}$ was designed so that the paddle wheel moves at maximum rotational velocity when the maximum energy, or maximum M_z , is seen from the results of the constant rotational velocity case 3. The phase angle of the sinusoidal function comes from a graphical approximation of the phase angle of case 3. This phase matching is done in an attempt to reduce fluctuations in the energy generated; the attempt is not significantly successful as can be seen in Fig. 8 but, interestingly, more power is generated. The sinusoidal rotational velocity does not increase the time required to reach a steady average power generation.

Table 2. Results from selected cases with variable rotational velocity.

Case	7	8
$C_{D,body}$	0.3104	0.3095
$C_{D,part}$	-0.0335	-0.0342
$C_{D,saved}$	0.0231	0.0248
$C_{D,power}$	336	359
$e_{capture}$	16.1	12.0

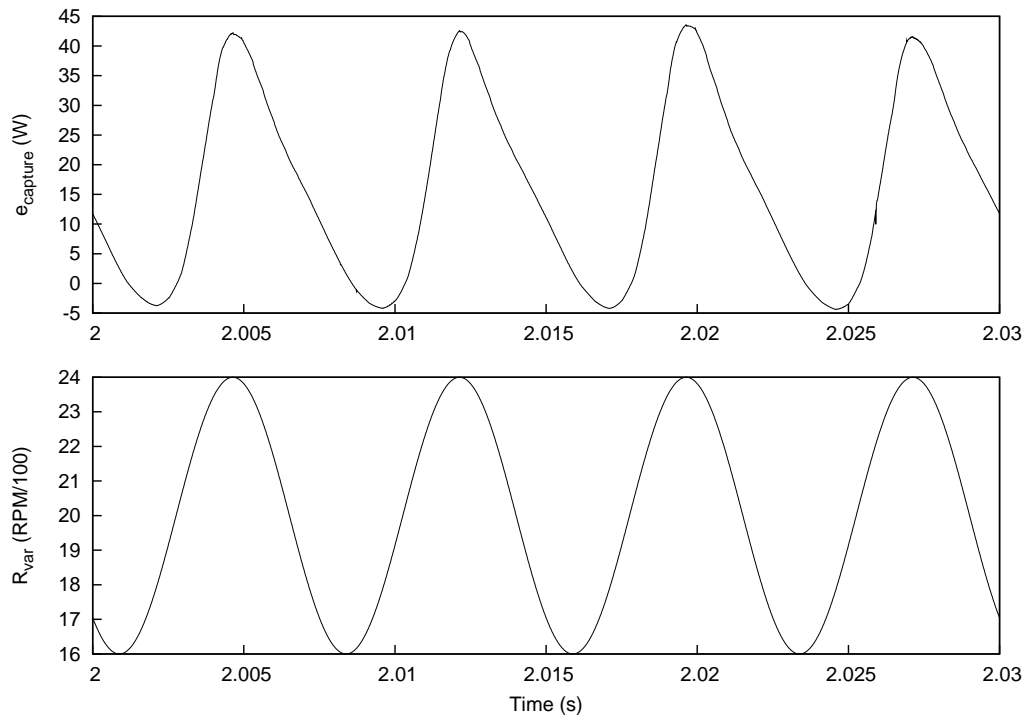
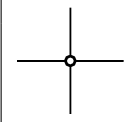
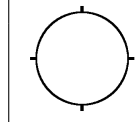
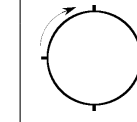
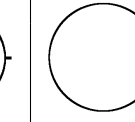
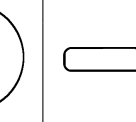


Figure 8. Plot of $e_{capture}$ and R vs Time for one full revolution of the paddle wheel from case 7.

5.2 Comparison cases

It is questioned whether the reduced drag is only due to the modification of the shape of the Ahmed model by the presence of the paddle wheel. Therefore, some cases of non-rotating paddle wheels and modified wheels are tested. Results of these cases are summarized in Tab. 3. The added parts have their center 13.3 cm behind the rear wall and 19 cm below the top wall and have a radius of 5 cm. Cases 0° and 30° model a fixed paddle wheel rotated by 0° and 30° from the horizontal position, respectively. Case A models a paddle wheel whose inner radius was enlarged to 0.045 m which makes it almost a cylinder. Case B is a copy of case A but the object revolves at 2500 RPM. Power consumed by the paddle wheel in case B is 1.28 watts. Case C is a 5 cm radius cylinder that does not rotate. Case D is an attempt at making the rear of the Ahmed body more streamline in order to compare the drag reduced by this streamline rear with the drag reduced by various wheel configurations. Graphical representations of the comparison cases are given in Tab. 3.

Table 3. Results from comparison cases.

Case	0°	30°	A	B	C	D
$C_{D,body}$	0.3111	0.3063	0.3099	0.3288	0.3107	0.2151
$C_{D,part}$	-0.0046	-0.0069	-0.0392	-0.0351	-0.0551	-
$C_{D,saved}$	-0.0065	0.0006	0.0292	0.0061	0.0445	0.0849
$C_{D,power}$	-94.5	8.8	445	87.9	645	1233
						

6. DISCUSSION

Several configurations of the paddle wheel are tested. The most power captured from the flow is seen in case 7 which models a 5 cm radius paddle wheel rotating at an average R of 2000 RPM, with R_{var} defined by Eq. (11); the power generated is 16.1 watts. The rotating paddle wheel configuration that reduces the drag coefficient the most is a paddle wheel rotating at roughly 4000 RPM, located slightly upwind of the maximum turbulent kinetic energy location, and having a radius of 4 cm. This drag reduction is followed closely by the variable angular velocity wheel of case 7.

Cases that let the flow cross the center of paddle wheel do not yield as much energy and are not documented in this paper; a filled center is deemed necessary because it serves to prevent incoming flow from being diverted between the paddles and wasting its kinetic energy. It is also noticed that the paddles should not interfere with the flow traveling outside of the separation bubble since doing so increases drag without increasing the amount of power generated.

Non-rotating paddle wheels do not reduce the drag coefficient; however, cases C and D reduce the total drag coefficient of the vehicle-cylinder assembly, which is an expected results because those modified cases present more streamlined bodies. It also reinforces the hypothesis that the paddle wheel creates a flow typical of a more streamlined body by its angular velocity and not by its shape. However, these cases are there for comparison only and are not the purpose of the paper; it is not the intent here to modify the shape of the car but rather to have an added part which generates energy and possibly reduces drag. By comparing the velocity streamlines of the reference case with those of the paddle wheel cases it is seen that the upper span-wise vortex is much smaller in presence of the rotating paddle wheel; this partly explains why the drag coefficient is reduced. Also, that vortex creates a suction on the paddle wheel and thus increases $C_{D,saved}$. There is visibly less turbulent kinetic energy in the cases with the paddle wheel, which indicates that less energy is lost by viscous dissipation.

From the analysis, it seems clear that R is highly influent on the energy output of the system. The best results are obtained at an average R of 2000 RPM. As expected, when the angular velocity of the paddle wheel reaches a certain value, the power generated turns into power that has to be fed to the wheel. On the other hand, for very low angular velocities the forces on the paddle wheel do not increase enough to compensate for the lower velocity of the wheel and thus the power generated decreases. When taking into account that a full revolution of the paddle wheel corresponds to four quarter cycles which are each geometrically identical, the fluctuations in energy captured and drag coefficient have the same period as the geometrical rotation of the paddle wheel; this is seen on Figs. 4 and 5. Four force cycles are noticeable for each complete revolution of the paddle wheel.

The flow modified by the rotating paddle wheel creates a vortex on the tip of the paddle every time it passes through the topmost point of the cycle. That vortex leaves the blade at a velocity greater than that of the paddle itself and is one of the two main forces driving the wheel, the other force being the large difference of pressure between the front and the back of the paddle when it goes through its bottommost point.

The fact that the best result comes from a variable rotational speed wheel shows that the energy capture can be adapted to the flow. The energy spent to accelerate and decelerate the mass of the paddle wheel for the variable rotational velocity cases was not considered into the calculation of $e_{capture}$ since it cancels itself out after each geometrical cycle and that power-generation and geometrical cycles have the same period. To have the angular velocity of the paddle wheel adapt to the flow, an algorithm where the angular velocity of the paddle wheel is a function of the forces that act on it is currently developed. Such a code would fit well with a paddle wheel that recaptures energy in the form of electricity because an electric motor can be controlled to regulate how much power is extracted from the paddle wheel. Gas-electric hybrid vehicles would suit as good candidates for such a system because they already have high capacity batteries on-board.

In the published literature, most of all Ahmed body analyses are ran with a fixed floor, and that is different from real-world situations where the floor has a relative velocity with respect to the car equal to the velocity of the car itself. This does not drastically modify the results but it was reported by Krajnovic and Davidson (2005) to have a 8% influence on the drag coefficient and a noticeable influence on the flow near the rear wall of the car. That zone is where this paper

is focused but the purpose here is to show how flow structures found on a typical car can be used to generate energy. Specific car models are not analyzed yet and the Ahmed body is only used as a model to create typical car flows and validate the calculations. The results obtained with the $k-\omega$ -SST model in two dimensions are fairly reasonable: the flow on the rear slant wall stays attached for the whole wall and a small low pressure zone appears at the onset of the slant wall; this compares well with the 25° experimental center-line flow which reattaches quickly, as reported by Guilmineau (2008). Moreover, Guilmineau noted that three-dimensional analyses with URANS model were not able to predict the reattachment on the rear slant wall.

Finally, it should be noted that more tests have to be run in order to yield results of greater energy capture and drag reduction. The authors believe that it is possible to get a positive energy capture to accompany results of large drag reduction given by the non-moving cylinder but that the good combination of rotational velocity and blade geometry has yet to be found.

7. CONCLUSION

It is found that the rotating paddle wheel can generate 16.1 watts while reducing drag by 7.7%. It can also reduce drag by 8.4% if power is supplied to the paddle wheel. This reduction is calculated from the extrapolation of two-dimensional simulations to a three-dimensional body. This extrapolation should hold as long as a device similar to what is reported by Beaudoin and Aider (2008) or by Lehugeur, Gilléron, and Ivanić (2006) is used to eliminate the influence of the stream-wise vortices on the span-wise vortices. Future plans include different blade shapes and flow driven rotational velocities. Finer and better suited meshes, three-dimensional analyses, and experimental tests are also considered for study.

8. ACKNOWLEDGEMENTS

We would like to thank all those who contributed to the development of OpenFOAM. We also recognize the ideas given by peers and the authors of various open-source programs used for our research.

9. REFERENCES

- Ahmed, S. R., Ramm, G. and Faltin, G., 1984, "Some salient features of the time averaged ground vehicle wake", Technical Report TP-840300, Society of Automotive Engineers, Warrendale, Pa., 31 p.
- Bayraktar, I., Landman, D. and Baysal, O., 2001, "Experimental and computational Investigation of Ahmed body for ground vehicle aerodynamics", SAE Transactions: Journal of Commercial Vehicles, Vol.110, No. 2, pp. 613-626.
- Bouris, D. and Bergeles, G., 1999, "2D LES of vortex shedding from a square cylinder", Journal of Wind Engineering and Industrial Aerodynamics, Vol.80, pp. 31-46.
- Beaudoin, J.-F. and Aider, J.-L., 2008, "Drag and lift reduction of a 3d bluff body using flaps", Experiments in Fluids, Vol.44, No. 4, pp. 491-501.
- Cousteix, J., 1989, "Turbulence et couche limite", Paris:Cépaduès Éditions, p. 166.
- Guilmineau, E., 2008, "Computational study of flow around a simplified car body", Journal of Wind Engineering and Industrial Aerodynamics, Vol.96, pp. 1207-1217.
- Hinterberger, C., García-Villalba, M. and Rodi, W., 2004, "Large Eddy Simulation of flow around the Ahmed body", Lecture Notes in Applied and Computational Mechanics, The Aerodynamics of Heavy Vehicles: Trucks, Buses, and Trains, Ed. R. McCallen, F. Browand and J. Ross, Springer Verlag, pp. 77-87.
- Krajnovic, S. and Davidson, L., 2005, "Influence of floor motions in wind tunnels on the aerodynamics of road vehicles", Journal of Wind Engineering and Industrial Aerodynamics, Vol.93, pp. 677-696.
- Lehuguer, B., Gilléron, P., Ivanić, T., 2006, "Contribution de l'éclatement tourbillonnaire à la réduction de la traînée des véhicules automobiles : approche numérique", C. R. Mécanique, Vol.334, pp. 368-372.
- Menter, F. and Esch, T., 2001, "Elements of industrial heat transfer predictions", Proceedings of the 16th Brazilian Congress of Mechanical Engineering, Vol.20, pp. 117-127.
- OpenCFD, 2008, "OpenFOAM user guide", Berkshire, UK.
- OpenCFD, 2009, "OpenFOAM-dev-1233 source code", Berkshire, UK.

10. Responsibility notice

The authors are the only responsible for the printed material included in this paper